CLM-P842

CLM-P842

A mathematical model of melt/water detonations

D. F. Fletcher
A. Thyagaraja

UK ATOMIC ENERGY AUTHORITY

Culham Laboratory

CLM-P842

A mathemetical model of melt/water detonations

D. F. Fletcher, A. Thyagaraja

Culham Laboratory, Abingdon, Oxon., OX14 3DB

ABSTRACT

In this paper we describe a new mathematical model of melt/water detonations. This model has been developed to study the escalation and propagation stages of a vapour explosion. After describing the physics of this problem we give a complete description of the conservation equations and constitutive relations which form the model. We then describe the the solution procedure and present some results from example simulations.

(Submitted for publication in Applied Mathematical Modelling)

July, 1988

Contents

Nomenclature

A	area factor
c_d	drag coefficient
c_{frag}	constant in the fragmentation model
c_v	specific heat at constant volume
e	internal energy
e_s	stagnation energy
h	heat transfer coefficient
h_s	stagnation enthalpy
K	momentum exchange function
L	length-scale
p	pressure
R	energy exchange function
T	temperature
t	time
V	velocity
x	axial coordinate or mass quality

Greek Symbols

α	volume fraction or void fraction
ρ	density
ν	specific volume ($= 1/\rho$)
Γ_f	mass transfer rate
Γ_{frag}	length-scale source term
Γ_v	Grüneisen coefficient
Δt	space step
Δx	time step

Subscripts

e	effective fluid (water plus fragments)
f	fragments
liq	saturated liquid
m	melt droplets
sat	saturation value
vap	saturated vapour
w	water

1 Introduction

If a hot liquid (melt) contacts a cooler volatile liquid, in some circumstances the energy transfer rate can be so rapid and coherent that an explosion results. Such explosions are a well-known hazard in the metal casting industry [1] and it is postulated that they may occur in submarine volcanisms [2]. They are also studied in the nuclear industry, to assess the consequences of the unlikely event that in a severe accident molten material contacts residual coolant and such an explosion results [3].

Explosions of this type are known to progress through a number of distinct phases [3]. Initially, the melt and water mix on a relatively slow timescale ($\sim$1 second). During this stage the melt and water zones have a characteristic dimension of the order of 10mm. Because of the high temperature of the melt a vapour blanket insulates the melt from the water and there is relatively little heat transfer. If this vapour blanket is collapsed in some small region of the mixture, high heat transfer rates result and there is a rapid rise in the pressure locally. In some circumstances this pressure pulse can cause further vapour film collapse and may escalate and propagate through the mixture, causing coherent energy release. The propagating pressure pulse (which steepens to form a shock wave) has two main effects. Firstly, it collapses the vapour blanket, initiating rapid heat transfer. Secondly, it causes differential acceleration of the melt and water, which in turn leads to relative velocity breakup of the melt and a large increase in the melt surface area. As the energy of the melt is rapidly transferred to the water high pressure steam is produced, which expands, with the potential to cause damage to any surrounding structures.

In earlier work we have developed a mathematical model, called CHYMES, of the mixing stage [4,5,6] and are in a position to predict what type of mixtures are formed in many different situations. In this paper we present a new mathematical model, called CULDESAC, of the detonation process. The analogy between thermal detonations and classical chemical detonations was first investigated in 1975 [7]. Since then a number of steady-state [8,9] and transient [10] models have been developed. We have improved upon this modelling by relaxing some of the assumptions which have, in the past, been made to make the problem tractable. We also have the benefit of a model of the mixing stage, which we can use to generate input data for the detonation model.

In section 2 of this paper we describe the partial differential equations which make up the model and the constitutive relations used to close it. In section 3 we describe the solution procedure and in section 4 we describe the results from some example calculations. Finally, in section 5 we draw some conclusions.

2 Description of the Model

In this section we describe the partial differential equations and constitutive relations which constitute the model. The model is transient and one-dimensional (although this may be planar, cylindrical, spherical or any user-specified slowly varying shape). We treat the mixture as consisting of melt particles, water and steam. Behind the detonation front the particles are fragmented by boundary layer stripping and the water is heated by energy transfer from the fragments. This situation is shown schematically in figure 1. In the model we represent this situation using three different components,

namely melt droplets (m), melt fragments (f) and water (w). Since the water is rapidly heated to supercritical pressures and temperatures we make the simplifying assumption that when distinct phases exist the steam and water are in thermal and mechanical equilibrium. We also assume that the melt fragment and water species are in mechanical equilibrium, which is reasonable since the melt fragments are very small ($\sim 100\mu m$) [11]. We assume that the fragmentation process is boundary layer stripping [12], although the model is sufficiently general to apply to any hydrodynamic fragmentation process. We have formulated this problem mathematically using the usual multiphase flow equations, where the presence of each species is specified by a volume fraction and all the species are at a common pressure. We make the simplifying assumption that the melt and fragments are incompressible, so that $\rho_f = \rho_m = constant$. Also since the water and the fragments are assumed to have the same velocity we set $V_f = V_w$.

2.1 Conservation Equations

Conservation of mass applied to the water, melt and fragments gives:

$$\frac{\partial}{\partial t}(\alpha_w \rho_w) + \frac{1}{A}\frac{\partial}{\partial x}(A\alpha_w \rho_w V_w) = 0 \tag{1}$$

$$\frac{\partial}{\partial t}(\alpha_m \rho_m) + \frac{1}{A}\frac{\partial}{\partial x}(A\alpha_m \rho_m V_m) = -\Gamma_f \tag{2}$$

and

$$\frac{\partial}{\partial t}(\alpha_f \rho_m) + \frac{1}{A}\frac{\partial}{\partial x}(A\alpha_f \rho_m V_w) = \Gamma_f. \tag{3}$$

In equations (2) and (3) Γ_f is the mass transfer rate due to fragmentation and is specified later.

Conservation of momentum for the melt and effective fluid, consisting of the water and the fragments, gives

$$\frac{\partial}{\partial t}(\alpha_m \rho_m V_m) + \frac{1}{A}\frac{\partial}{\partial x}(A\alpha_m \rho_m V_m^2) =$$

$$-\alpha_m \frac{\partial p}{\partial x} + K_{mw}(V_w - V_m) - \Gamma_f V_m \tag{4}$$

and

$$\frac{\partial}{\partial t}((\alpha_w \rho_w + \alpha_f \rho_m)V_w) + \frac{1}{A}\frac{\partial}{\partial x}(A(\alpha_w \rho_w + \alpha_f \rho_m)V_w^2) =$$

$$-(\alpha_w + \alpha_f)\frac{\partial p}{\partial x} + K_{mw}(V_m - V_w) + \Gamma_f V_m. \tag{5}$$

The terms on the RHS of equations (4) and (5) represent the effect of the pressure gradient force, drag between the melt particles and an effective fluid, consisting of the water plus the fragments, and momentum transfer due to mass transfer. Viscous forces have been ignored, since they are always negligible in situations of interest to us.

We also have an energy equation for each species. It is convenient to work in terms of the stagnation energy, defined by $e_s = e + 1/2V^2$ and the stagnation enthalpy defined by $h_s = e_s + p/\rho$. Conservation of energy for the melt, fragments and water gives:

$$\frac{\partial}{\partial t}(\alpha_m \rho_m e_{sm}) + \frac{1}{A}\frac{\partial}{\partial x}(A\alpha_m \rho_m V_m h_{sm})$$

$$= -p\frac{\partial \alpha_m}{\partial t} + R_{mw}(T_w - T_m) + V_m K_{mw}(V_w - V_m) - \Gamma_f h_{sm} \tag{6}$$

$$\frac{\partial}{\partial t}(\alpha_f \rho_m e_{sf}) + \frac{1}{A}\frac{\partial}{\partial x}(A\alpha_f \rho_m V_w h_{sf})$$
$$= -p\frac{\partial \alpha_f}{\partial t} + R_{fw}(T_w - T_f) + \Gamma_f h_{sm} \tag{7}$$

and

$$\frac{\partial}{\partial t}(\alpha_w \rho_w e_{sw}) + \frac{1}{A}\frac{\partial}{\partial x}(A\alpha_w \rho_w V_w h_{sw})$$
$$= -p\frac{\partial \alpha_w}{\partial t} + R_{mw}(T_m - T_w) + R_{fw}(T_f - T_w)$$
$$+V_w K_{mw}(V_m - V_w) + K_{mw}(V_w - V_m)^2. \tag{8}$$

In the above equations the terms involving R_{mw} etc. represent thermal equilibration and the terms containing K_{mw} are the drag work. We have assumed that all the irreversible drag work heats up the water. A detailed derivation of these equations is given elsewhere [13].

We also have an equation for the length-scale of the melt droplets, given by:

$$\frac{\partial}{\partial t}(\alpha_m \rho_m L_m) + \frac{1}{A}\frac{\partial}{\partial x}(A\alpha_m \rho_m V_m L_m) = -\Gamma_f L_m - \Gamma_{frag}. \tag{9}$$

In the above equation the term involving Γ_f is due to mass transfer (it is a consequence of writing the transport equation in conservation form) and the term $-\Gamma_{frag}$ models the chosen fragmentation process.

In addition to the above equations we have the constraint that

$$\alpha_m + \alpha_f + \alpha_w = 1. \tag{10}$$

This completes the specification of the differential equations. In the next subsections we will describe the constitutive relations, the Equations of State (EOS) and the boundary and initial conditions.

2.2 Constitutive Relations

In this section we describe the constitutive relations for drag, heat transfer and fragmentation currently employed in the model. These may be changed very easily as improved data becomes available.

2.2.1 Momentum Exchange

If the volume fraction of droplets is α_m there are $6\alpha_m/\pi L_m^3$ spherical droplets per unit volume. The drag force on a single droplet may be written as

$$F_D = \frac{1}{2}c_d \rho_e \pi \frac{L_m^2}{4}|V_w - V_m|(V_w - V_m) \tag{11}$$

where $\rho_e = (\alpha_w \rho_w + \alpha_f \rho_f)/(\alpha_w + \alpha_f)$ is the effective density of the fluid dragging the melt drops. Thus the total drag force is

$$F_T = \frac{3}{4}\frac{c_d}{L_m}\rho_e \alpha_m |V_w - V_m|(V_w - V_m) \tag{12}$$

and comparison of equation (12) with equation (4) shows that

$$K_{mw} = \frac{3}{4} c_d \alpha_m \frac{\rho_e}{L_m} |V_w - V_m| \tag{13}$$

In the present work we have used a constant value of $c_d = 2.5$. This value is higher than the usual value of 0.4 to account for the increased drag when drops are fragmenting [12]. It is a simple matter to make c_d a function of the volume fractions etc., if required.

2.2.2 Heat Transfer

If the heat transfer rate is specified as the product of a heat transfer coefficient and the temperature difference it is easily shown that

$$R_{mw} = 6\alpha_m \frac{h_{mw}}{L_m} \tag{14}$$

and

$$R_{fw} = 6\alpha_f \frac{h_{fw}}{L_f} \tag{15}$$

where h_{mw} is the heat transfer coefficient between the melt and water, h_{fw} is the heat transfer coefficient between the fragments and water and L_f is the fragment size. The heat transfer mechanisms between the melt and water are very complex and clearly depend on the time-history of each particle. The only experimental data available is rather crude and consists of time-averaged heat transfer coefficients for the duration of the fragmentation process [14]. Thus in the present model we have decided to choose constant values for the heat transfer coefficients. A value of $h_{mw} = 10^3\ W/m/K$ was used for the melt when it was surrounded by a vapour film. This is a typical value obtained from a combination of radiation and film boiling [14]. This value was increased by typically four orders of magnitude when vapour film collapse was judged to have occurred. The treatment of vapour film collapse used here was simply to increase the heat transfer coefficient when the pressure exceeded a certain value, since this models pressure induced vapour film collapse. Because of the high initial temperature of the melt ($\sim 2500K$) in situations of interest to us, temperature controlled vapour film collapse was not considered to be important [15].

The fragment size L_f is not determined by the fragmentation model currently employed (see section 2.2.3) and was specified by reference to experimental data. A typical value of $L_f = 100\mu m$ was used [11].

2.2.3 Fragmentation Model

As already mentioned we have chosen to use a boundary layer stripping model for fragmentation as this is thought to be the most appropriate for the study of vapour explosions [10]. We have used the model proposed by Carachalios et al. [10], who suggest that the stripping rate from a single fragment is given by

$$\frac{dm}{dt} = c_{frag} |V_m - V_w| \pi L_m^2 \sqrt{\rho_m \rho_e} \tag{16}$$

where the empirical constant c_{frag} takes a value of approximately 1/6. Multiplying equation (16) by the number of drops per unit volume and comparing the result with equation (2) gives

$$\Gamma_f = \alpha_m c_{frag} |V_m - V_w| \sqrt{\rho_e \rho_m} / L_m \tag{17}$$

where all the constant terms have now been included in c_{frag}, so that $c_{frag} \sim 1$. Thus the mass stripping rate is proportional to the relative velocity and the square root of the effective density. As fragmentation occurs, the density of the surrounding fluid is increased by the addition of fragments and thus the fluid has more inertia to fragment the drops further.

The length-scale of the droplets is changed by the mass loss due to boundary layer stripping. For spherical drops it is easily shown that the mass loss rate given in equation (17) implies a length-scale source term of

$$\Gamma_{frag} = \frac{1}{3} \Gamma_f L_m \tag{18}$$

which is not surprising, as equation (18) implies that a droplets length-scale changes at one third the rate of its volume. We have also added an empirical function of our own to ensure that breakup only occurs for Weber numbers above a critical value ($We_{crit} \approx 12$). Details are given in reference 16.

2.3 Equations of State

The melt equation of state is very easy. We assume the melt to be incompressible so that $\rho_m = \rho_f = constant$ and to have a simple caloric equation of state so that $E_m = c_{vm} T_m$ and $E_f = c_{vm} T_f$. (This EOS is easily modified to take account of the latent heat of fusion, although it is simpler to increase c_{vm} to account for this [14].)

The EOS for water is more complicated and there is virtually no thermodynamic data on the properties of water at high temperature and pressures. In this study we have used an approximate EOS, which will be described below. Before doing this it is important to determine exactly what form of EOS is needed in the calculation. We show, in section 3, that at the end of each time-step the water mass conservation equation gives the new density and the water energy equation the new internal energy. Thus from the EOS we need to determine the pressure and the temperature. The procedure used depends on whether the given values of ρ and e locate a point inside or outside of the two-phase region. Given ρ, a look-up table is used to determine whether $e > e_{sat}$ and the point is outside the two-phase envelope or $e \leq e_{sat}$ and the point is inside the two-phase region.

If it is inside the two-phase region then there exists x (the mass quality) such that

$$\nu = x\nu_{vap} + (1 - x)\nu_{liq} \tag{19}$$

and

$$e = xe_{vap} + (1 - x)e_{liq} \tag{20}$$

where ν is the specific volume and the suffices vap and liq refer to values on the vapour and liquid saturation lines, respectively. If x is eliminated between equations (19) and (20) we obtain an equation for p, since ν_{vap}, ν_{liq} etc. are a function of only one

thermodynamic variable. This equation is solved by the bisection method to determine the pressure and hence the temperature. Test calculations showed that for a look-up table containing 40 data points, this algorithm reproduces steam table data with an error of less than 0.5%.

Outside of the the two-phase region the pressure is obtained using a Grüneisen EOS [17], which gives:

$$p = p_{sat} + \Gamma_v \rho (e - e_{sat}) \tag{21}$$

where p_{sat} and e_{sat} are the saturation pressure and internal energy for a density ρ and Γ_v is the Grüneisen coefficient, which is assumed to be a function of the density only. This type of EOS is often used to determine the pressure at points removed from a reference line, given data along the reference line (often a shock adiabatic) [17]. Due to a lack of experimental data Γ_v was set to a constant value of 0.3. The temperature is given by

$$T = T_{sat} + (e - e_{sat})/c_v \tag{22}$$

where c_v is the specific heat at constant volume. A constant value of 3000 J/kg/K was used for the specific heat. (The Grüneisen approximation requires that all quantities are a function of volume only but thermodynamic consistency relations show that c_v can be a function of temperature only, hence c_v must be a constant.) This EOS was also tested against the (limited) data available from steam tables and was found to give results which were in agreement to within approximately 10% for both the pressure and temperature. This is perfectly adequate given the other uncertainties in the model.

2.4 Boundary and Initial Conditions

We are interested in solving the above equations in a closed vessel. Thus the only boundary condition needed is to set the velocities to zero at the vessel walls.

Initially, the volume fractions, void fraction, velocity and particle size distribution are specified. To simulate triggering some of the melt is fragmented in a small region of the solution domain. This causes a high heat transfer rate in these cells, the pressure rises locally and a detonation wave may develop.

3 Solution Procedure

We solve the partial differential equations using a finite difference method which employs the usual staggered grid arrangement. All convective terms are modelled using upwind differencing for stability. As far as possible we use explicit methods, where appropriate treating source terms implicitly, to ensure that positive quantities remain positive [18]. A version of the scheme, used to model detonations in gas mixtures, is described in [19] and its extension to multiphase flow is described in [13,20]. A brief summary of the solution procedure as it applies to this problem will be given below.

1. Equations (1), (2) and (3) are used to time advance $\alpha_w \rho_w$, α_m and α_f, respectively. Equation (10) is then used to determine α_w and hence ρ_w can be determined.

2. Equations (4) and (5) are used to obtain the new velocity fields. The drag and mass transfer terms are treated implicitly and the convection and pressure gradient terms are treated explicitly. Thus at each point a 2×2 matrix is inverted to obtain both velocities simultaneously. This practice has proved to be very stable.

3. The new stagnation energies are found by time advancing the three energy equations (6) $\rightarrow$ (8). Using the stagnation form ensures that the Rankine-Hugoniot equation can be built into the solution scheme to give it good shock-capturing properties. The new velocity field is then used to determine the new internal energies.

4. The caloric equations are used to determine the new melt and fragment temperature. The water EOS is then used to determine the new pressure field and the water temperature.

This completes a cycle of the solution procedure.

4 Example Simulations

We have used versions of this model to study shocks and detonations in gas mixtures [19], shocks and detonations in multiphase mixtures [13, 21] and shocks in dusty and droplet laden gases [16]. In all cases we have obtained excellent agreement with analytic theory, provided that we ensure that the spatial and temporal discretization is adequate to resolve the important physical processes [20,21] e.g. to obtain an accurate solution all the energy must not be released in a single cell.

4.1 Description of the Calculations

In this section we describe the parameters and initial conditions used in the simulations. Table 1 contains a list of all the parameters not specified in the earlier sections. All the simulations were started by assuming that there was a spatially uniform mixture with a specified melt volume fraction and void fraction. This mixture was assumed to be at rest. An explosion was triggered by instantaneously fragmenting 90% of the melt in the first 0.01m adjacent to the right-hand wall (or centre in the case of the cylindrically and spherically symmetric simulations). In the next subsections we will describe the results of simulations performed to study the effect of varying the initial void fraction of the water, the geometry and the heat transfer rate.

4.2 The effect of Void Fraction

In this section we present the results of three simulations performed in order to study the effect of void fraction on the escalation/detonation behaviour. Values of the void fraction (the fraction of the water in vapour form) of 0.5, 0.7 and 0.9 were used in the simulations. (The time-step was reduced by a factor of 10 in the $\alpha = 0.5$ case because of the lower compressibility of the water-steam mixture.) Figures 2(a)-(e) show the volume fraction, water density, pressure, temperature and velocity profiles as a function of distance after 0.8ms for the $\alpha = 0.7$ case. Figure 2(a) shows that the

Parameter	Value	unit
Time-step	10^{-7}	s
Space-step	0.005	m
Initial particle size	0.005	m
Initial pressure	0.1	MPa
Heat transfer rate - vapour blanketed	10^3	W/m/K
Heat transfer rate - liquid-liquid contact	10^7	W/m/K
Pressure required to collapse vapour blanket	0.2	MPa
Initial melt temperature	2500	K
Melt density	7000	kg/m^{-3}
Melt heat capacity	500	J/kg/K
Melt surface tension	0.4	N/m
Initial melt volume fraction	0.1	-

Table 1: Parameters used in the detonation simulations

melt is rapidly fragmented and that the fragments tend to follow the detonation front. Figures 2(b) and 2(c) show the rapid rise in density and pressure at the shock front, with the characteristic Von Neumann spike evident. Behind the detonation front the pressure and density fall and attain a constant value in the downstream region. Figure 2(d) shows the rapid heating of the water as the fragments are formed and transfer their energy to the water. Both the melt and fragments equilibrate their temperatures quickly with the water. The temperature behind the detonation front is seen to be in the supercritical region. Finally, figure 2(e) shows the velocity profiles. The water velocity profile is that characteristic of flow which is induced by a shock wave, showing a very steep rise at the shock front. The melt velocity rises more slowly, as the melt particles have more inertia. The large velocity difference which results causes very rapid fragmentation, as shown in figure 2(a).

Figures 3, 4 and 5 show the development of the pressure profile for initial void fractions of 0.5, 0.7 and 0.9, respectively. (Predicted pressure fields are displayed since they are often the only diagnostic data available from experiments.) The figures show that the shape of the pressure profile is very different in the three different cases. The higher the void fraction the more compressible the water/steam mixture and consequently the less 'spiky' the pressure plot. This is because high density water has a very high sound speed so that small changes in density cause very large changes in the pressure. In the two higher void fraction cases there is sufficient vapour present to stop the thermodynamic trajectory of the water ever entering the subcooled liquid region, where the sound speed is very high. There is also a physical instability in the pressure at the shock front which is present in the $\alpha = 0.5$ case. We will describe and explain this in subsection 4.4.

Table 2 compares the main features of the different simulations. The results in table 2 show that the detonation velocity, peak pressure and wall pressure (the pressure at $x = 0$) are all very sensitive to the void fraction. The detonation velocity increases

Case	Detonation speed (m/s)	Peak Pressure (MPa)	Wall Pressure (MPa)
0.5	580	160	25
0.7	725	285	60
0.9	770	210	74

Table 2: The effect of Initial Void Fraction

Case	Detonation speed (m/s)	Peak Pressure (MPa)	Wall Pressure (MPa)
Planar	725	285	60
Cylindrical	670	250	50
Spherical	645	230	48

Table 3: The effect of Geometry

with void fraction. The peak pressure is a maximum for the $\alpha = 0.7$ case and falls if there is either too much or too little water. The downstream pressure increases monotonically with void fraction. This is because in all cases the shock wave is strong enough to cause complete fragmentation of the melt, so that the final pressure is that corresponding to the 'mixing-cup' temperature for the melt and water, since figure 2(e) shows that the system is at rest in this region of the tube. Note that the pressures at the wall are super-critical and that the model predicts extremely high shock pressures. This is a consequence of assuming a 1D planar geometry and using parameters which ensure complete fragmentation of the melt.

4.3 The effect of Geometry

In this section we describe the results from two further calculations carried out to examine the effect of geometry. We have repeated the $\alpha = 0.7$ calculation described above for the cases of cylindrically and spherically symmetric detonations. These cases were simulated by changing the factor A in the conservation equations from a constant value to x and x^2, respectively. The resulting pressure profiles are shown in figures 6 and 7 respectively. The figures show that changing from a planar geometry reduces the peak pressures and the detonation velocity. Table 3 summarises this data. Note that the final pressure is somewhat reduced in the cylindrical and spherical cases because more of the energy is in the form of kinetic energy. We may conclude from this data that although the geometry affects the propagation behaviour, its effect is not great for the chosen initial conditions and coarse mixture.

4.4 The effect of the Heat Transfer Rate

In this section we present the results from simulations carried out in order to examine the effect of varying the heat transfer rate. We use these results to explain the oscillations in the pressure profiles for the $\alpha = 0.5$ simulation shown in figure 3. Figure 8 shows the results of a simulation performed with identical parameters to that shown in figure 4, except that the heat transfer rate was reduced by a factor of 10. A number of

features are evident from the figure. Firstly, the detonation takes longer to develop to a steady-state condition, as expected. The detonation velocity, effective peak pressure (marked by the dotted line) and wall pressure are very similar in both cases. The pressure peak is wider in figure 8, because the heat transfer zone is longer.

The second point to note is that there are short-lived oscillations superimposed on the pressure peak. These are very similar to those seen in figure 3. These are due to the reduced heat transfer rate behind the front, causing rapid pressure variations to occur. Because the heat transfer is reduced the temperature of the water increases less rapidly and remains close to its saturation value in a small region behind the shock front. Equations (21) and (22) can be combined to give

$$p = p_{sat} + \gamma_v (T - T_{sat}) \tag{23}$$

where $\gamma_v = \rho \Gamma_v c_v$ is the thermal pressure coefficient. From the data given in section 2.3 we see that a typical value of γ_v is 10^6 (MPa/K). Thus if the temperature remains close to its saturation value it is possible for a small change in $T - T_{sat}$ to cause a large change in the pressure relative to p_{sat}. This is a consequence of $\gamma_v (T_{crit}/p_{crit})$ being large (~ 30). If the heat transfer rate is high the water is soon heated above its critical temperature. In this case both p_{sat} and T_{sat} are negligible and this phenomenon disappears. A simulation with the heat transfer rate lowered by a further factor of 10 produced a very slowly developing detonation with many oscillations at the shock front.

These oscillations do not appear to have any dynamical significance. The detonation tends to develop a steady-state structure with the small oscillations superimposed on it. In the void fraction study, reducing the void fraction decreases the internal energy of the water and consequently more energy must be added to the water before its temperature is raised to a supercritical value. Similar oscillations to those observed here were observed by Fishlock [22] in a study of detonation in melt/sodium systems, using the same form of EOS as used here. He was unable to explain the origin of these oscillations and assumed that they were due to numerical instability. We have checked that they do not disappear when the grid is refined and the time-step is reduced. (Although they can be removed by increasing Δx so that the 'hot' and 'cold' regions are averaged out.) Note that the finite difference grid and the time-step were the same for the calculations presented in figures 4 and 5 and that a *reduction* in the energy source term causes greater 'spikeness'. Hence it cannot be a numerical effect. (We do not encounter any numerical instability if the proper Courant restrictions are observed for Δt and Δx). It is not clear whether this behaviour is a consequence of the chosen form of the EOS or a genuine property of detonations in near saturated water. However, since its effect is limited to adding short-lived transients to the solution it appears to be of little practical importance.

5 Conclusions

In this paper we have described a new model of melt/water detonations. The model uses the usual multiphase flow equations to simulate the passage of a detonation wave through a mixture of melt and water. The model assumes that differential acceleration of the melt and water, by the passage of a shock front, causes relative velocity induced

fragmentation of the melt. This fragmentation, together with the collapse of the vapour blanket, leads to the development of a detonation wave. In this work we do not fit a shock wave at the detonation front or assume steady-state propagation but calculate the response of the system given an initial disturbance. Thus we can examine the *development* of detonations from a simulated trigger.

We have presented example calculations which illustrate the structure of the detonation front, as well as the effect of the initial void fraction and geometry on the detonation process. It is evident from the description of the model that there are many parameters, both in the initial conditions and in the constitutive relations, which are either uncertain or depend on the prescribed coarse mixture. In future work we plan to determine which are the most important parameters and to map out the region in α_m, α, D_m space which can be considered as good mixtures. We also plan to compare model predictions with experimental data, if any suitably detailed data can be found.

Acknowledgements

This work was funded by the General Nuclear Safety Research (GNSR) Programme.

References

[1] G. Long, *Explosions of molten metal in water - causes and prevention.* Metals progress, **71**, 107-112, (1957).

[2] S.A. Colgate and T. Sigurgeirsson, *Dynamic mixing of water and lava.* Nature, **244**, 552-555, (1973).

[3] A.W. Cronenberg, *Recent developments in the understanding of energetic molten fuel coolant interaction.* Nucl. Safety, **21**, 319-337, (1980).

[4] A. Thyagaraja and D.F. Fletcher, *Buoyancy-driven, transient, two-dimensional thermo-hydrodynamics of a melt-water-steam mixture.* Comput. Fluids, **16**, 59-80, (1988).

[5] D.F. Fletcher and A. Thyagaraja, *Numerical simulation of two-dimensional transient multiphase mixing.* Proc. 5th Int. Conf. on Numerical Methods in Thermal Problems, Montreal, Canada, June 29th - July 3rd 1987, **V**(2), 945-956, Pineridge, (1987).

[6] D.F. Fletcher and A. Thyagaraja, *A method of quantitatively describing a multi-component mixture.* PhysicoChem. Hydrodynam., **9**, 621-631, (1987).

[7] S.J. Board, R.W. Hall and R.S. Hall, *Detonation of fuel coolant explosions.* Nature, **254**, 319-321, (1975).

[8] R.W. Hall and S.J. Board, *The propagation of large scale thermal explosions.* Int. J. Heat Mass Transfer, **22**, 1083-1093, (1979).

[9] A. Sharon and S.G. Bankoff, *On the existence of steady supercritical plane thermal explosions.* Int. J. Heat Mass Transfer, **24**, 1561-1572, (1981).

[10] C. Carachalios, M. Burger and H. Unger, *A transient two-phase model to describe thermal detonations based on hydrodynamic fragmentation.* Proc. Int. Meeting on LWR severe accident evaluation, Cambridge, Massachusetts, 28 August - 1 September, (1983).

[11] D.F. Fletcher, *The particle size distribution of solidified melt debris from molten fuel-coolant interaction experiments.* Nucl. Engng. Des., **105**, 313-319, (1988).

[12] M. Pilch and C.A. Erdman, *Use of breakup time data and velocity history data to predict the maximum size of stable fragments for acceleration-induced breakup of a liquid drop.* Int. J. Multiphase Flow, **13**, 741-757, (1987).

[13] D.F. Fletcher and A. Thyagaraja, *Multiphase flow simulations of shocks and detonations, Part I: Mathematical formulation and shocks.* Culham Laboratory Report: CLM-R279, (1987).

[14] D.F. Fletcher, Modelling transient energy release from molten fuel coolant interaction debris. AEE Winfrith Report: AEEW-M2125, (1984).

[15] T.A. Dullforce, D.J. Buchanan and R.S. Peckover, *Self-triggering of small-scale fuel-coolant interactions: 1. experiments.* J. Phy. D. Appl. Phys., 9, 1295-1303, (1976).

[16] D.F. Fletcher and A. Thyagaraja, *Multiphase flow simulations of shocks and detonations, Part III: Droplet laden gas flows.* Culham Laboratory Report: CLM-R283, (1988).

[17] S. Eliezer, A. Ghatak, H. Hora and E. Teller, *An introduction to equations of state: theory and applications.* CUP, Cambridge, (1986).

[18] A. Thyagaraja, D.F. Fletcher and I. Cook, *One dimensional calculations of two-phase mixing flows.* Int. J. Numer. Methods Eng., **24**, 459-469, (1987).

[19] D.F. Fletcher and A. Thyagaraja, *Some calculations of shocks and detonations for gas mixtures.* Culham Laboratory Report: CLM-R276, (1987). (To appear in Computers and Fluids.)

[20] D.F. Fletcher and A. Thyagaraja, *Multiphase flow—a self-consistent approach.* Paper presented at the ICFD conference on Numerical Methods for Fluid Dynamics, 21-24 March, 1988. (Proceedings to appear.)

[21] A. Thyagaraja and D.F. Fletcher, *Multiphase flow simulations of shocks and detonations, Part II: Detonations.* Culham Laboratory Report: CLM-R280, (1987).

[22] T.P. Fishlock, Private Communication.

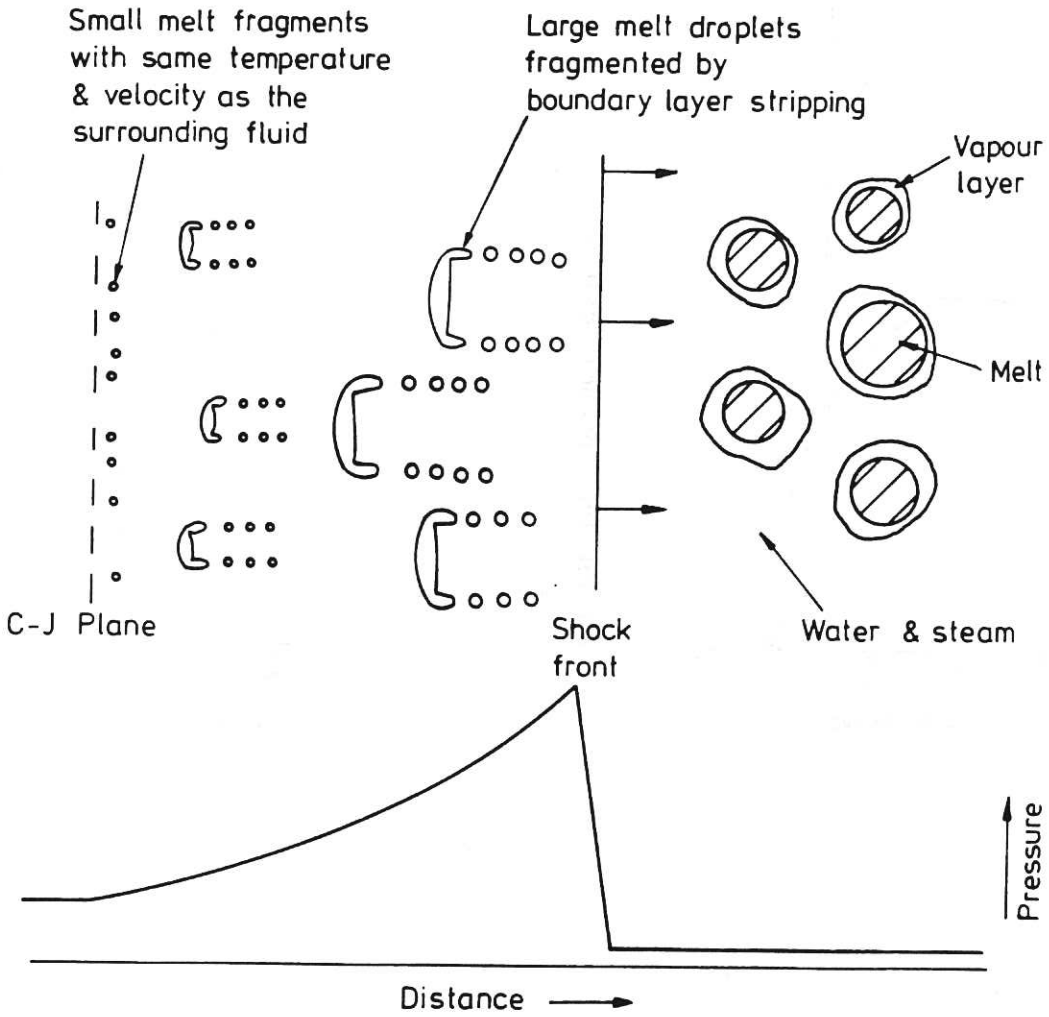

Fig. 1 Schematic representation of a detonation front in a melt/water mixture

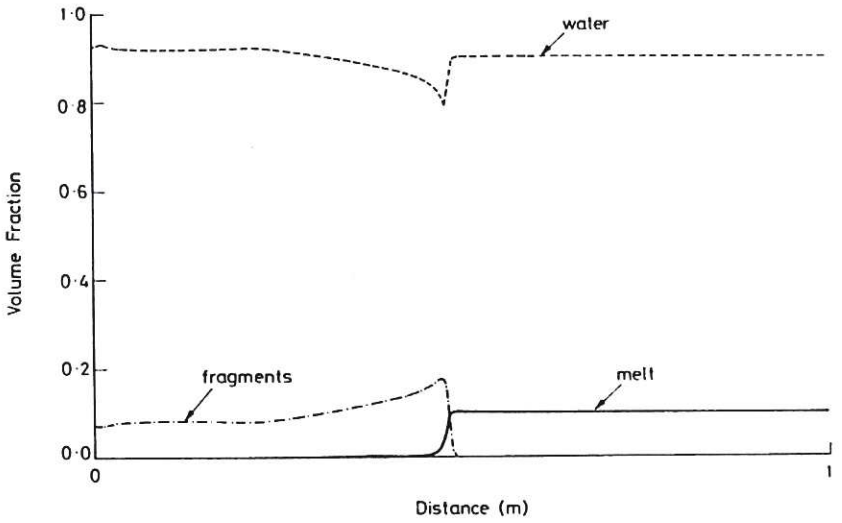

Fig. 2(a) Volume fraction profiles for $a=0.7$ case

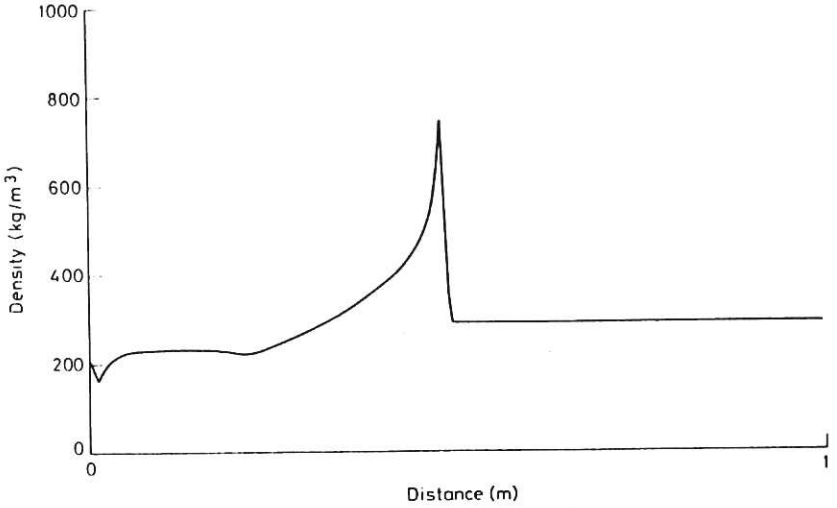

Fig. 2(b) Density profile for $a=0.7$ case

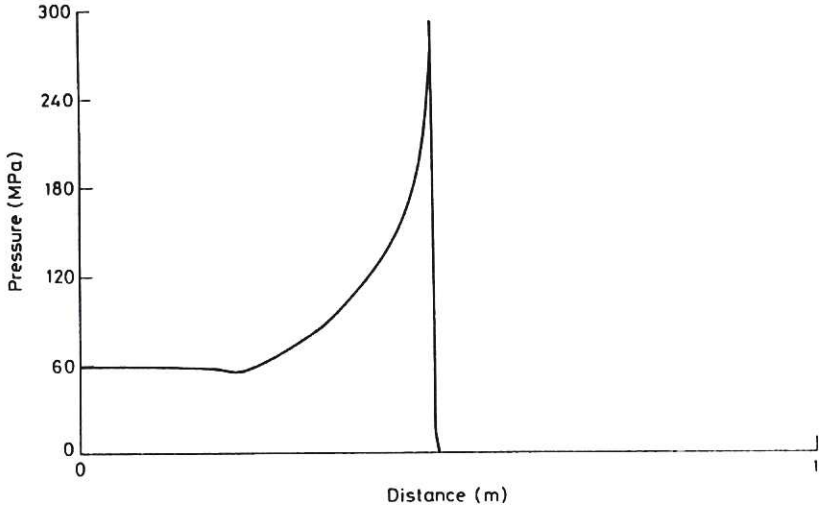

Fig. 2(c) Pressure profile for $a=0.7$ case

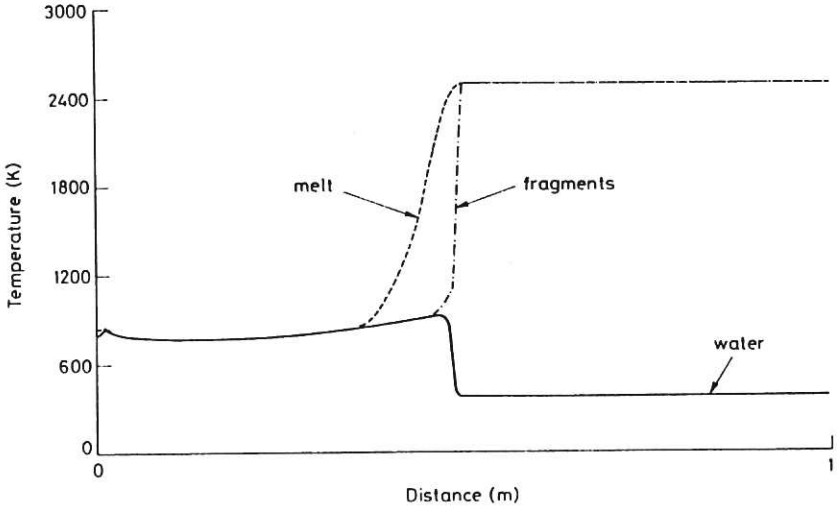

Fig. 2(d) Temperature profiles for $a=0.7$ case

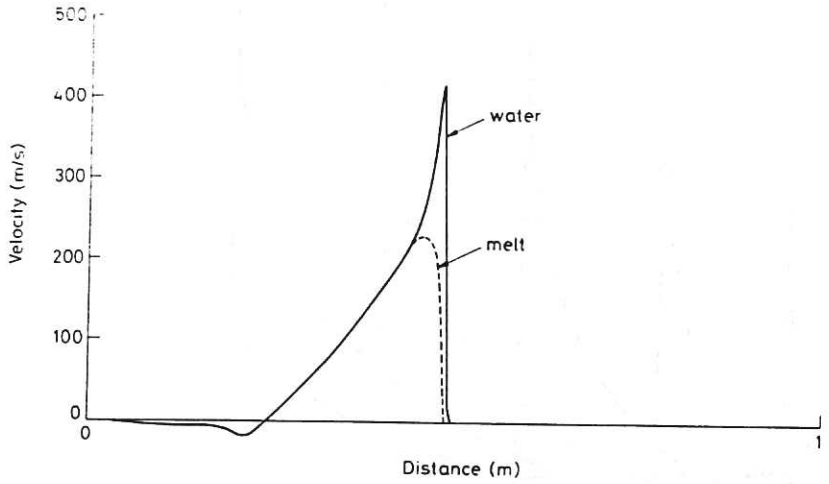

Fig. 2(e) Velocity profiles for $a=0.7$ case

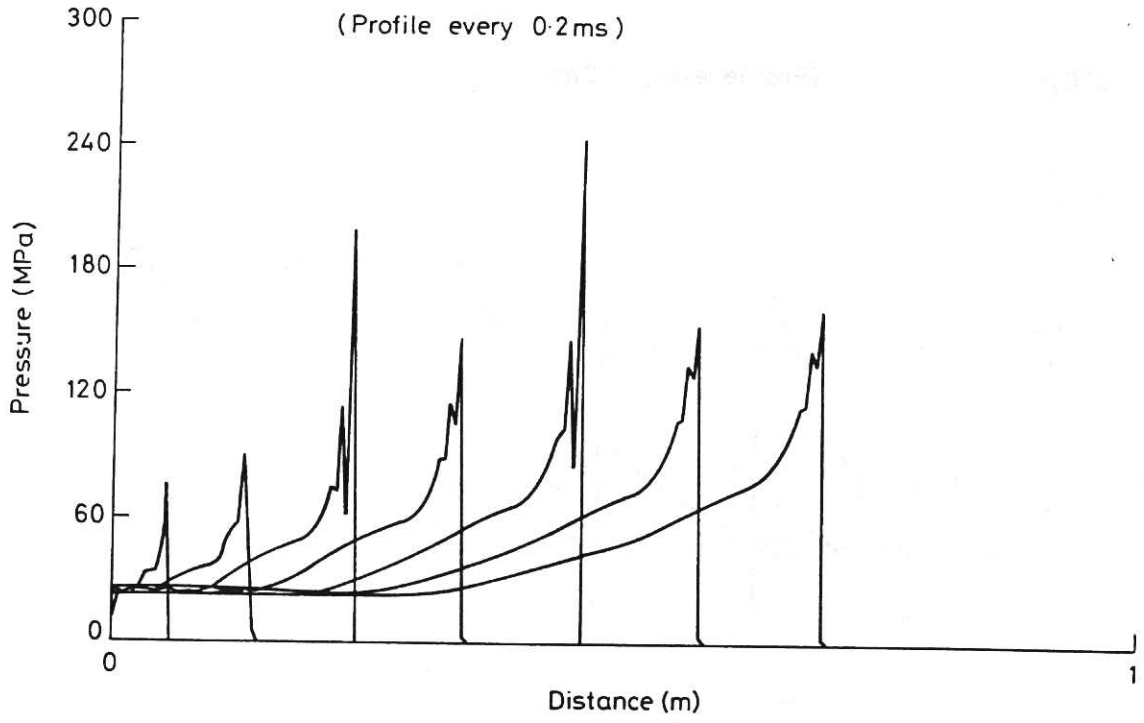

Fig. 3 Development of the pressure profile for $a=0.5$ case

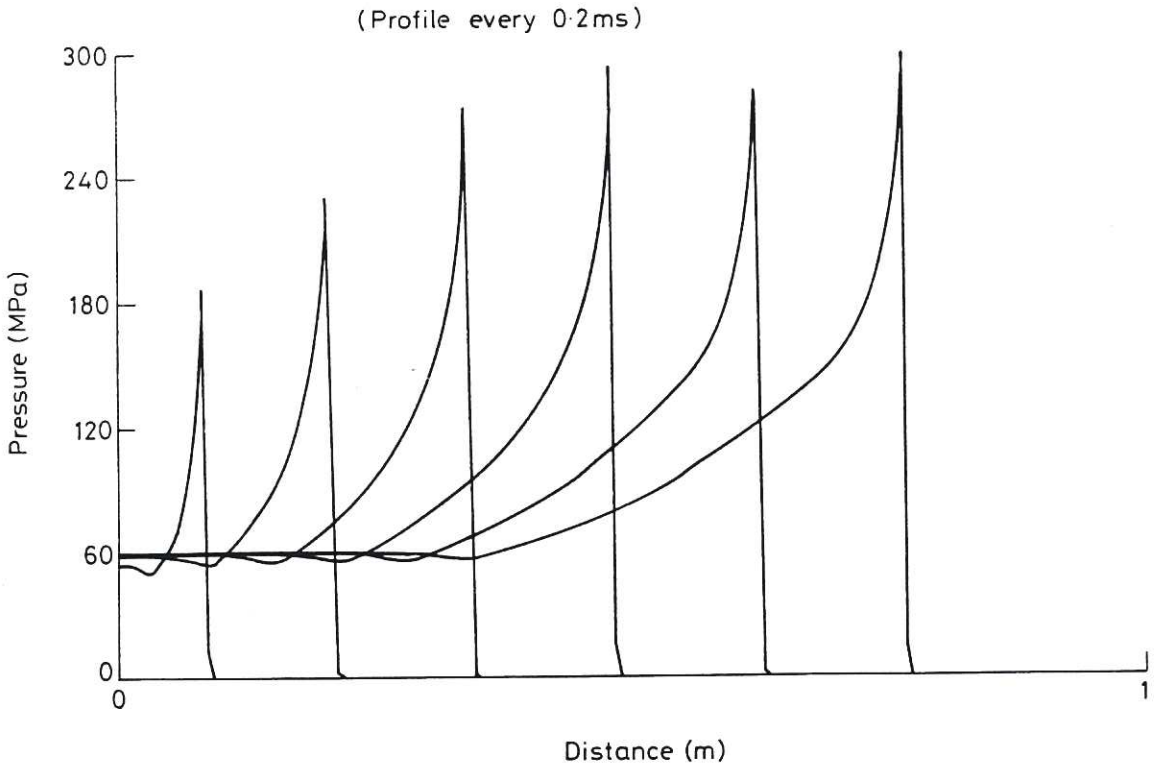

Fig. 4 Development of the pressure profile for $a=0.7$ case

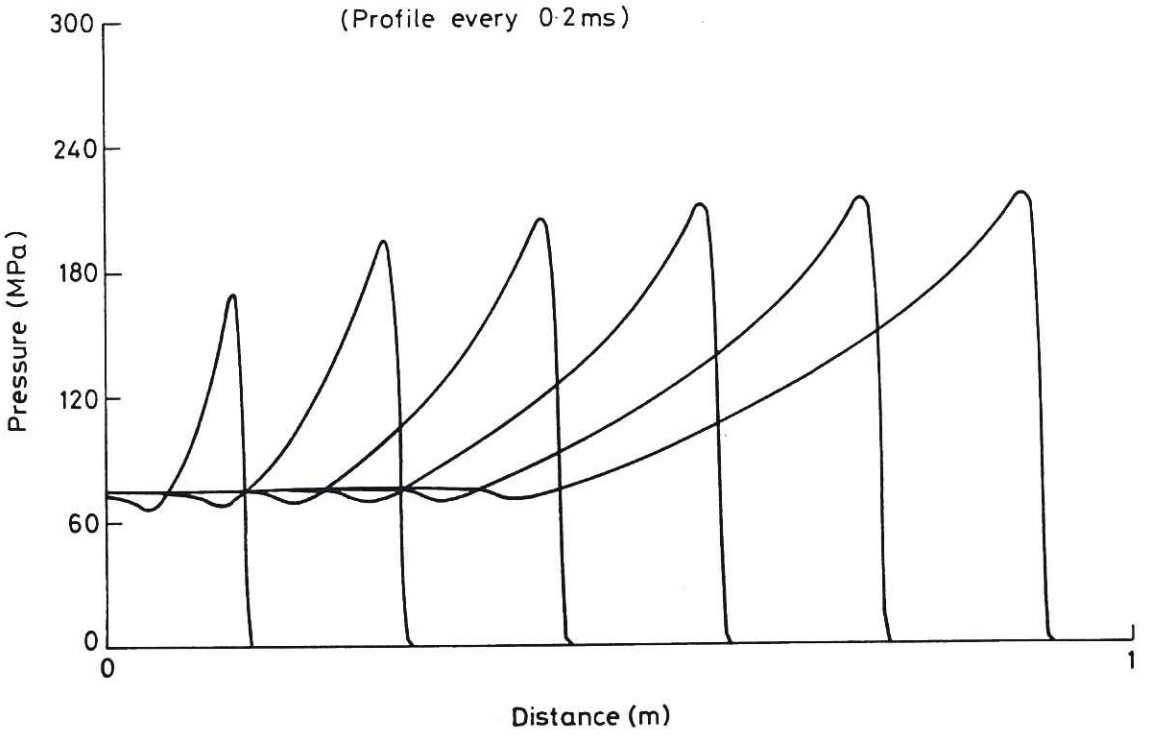

Fig. 5 Development of the pressure profile for $a=0.9$ case

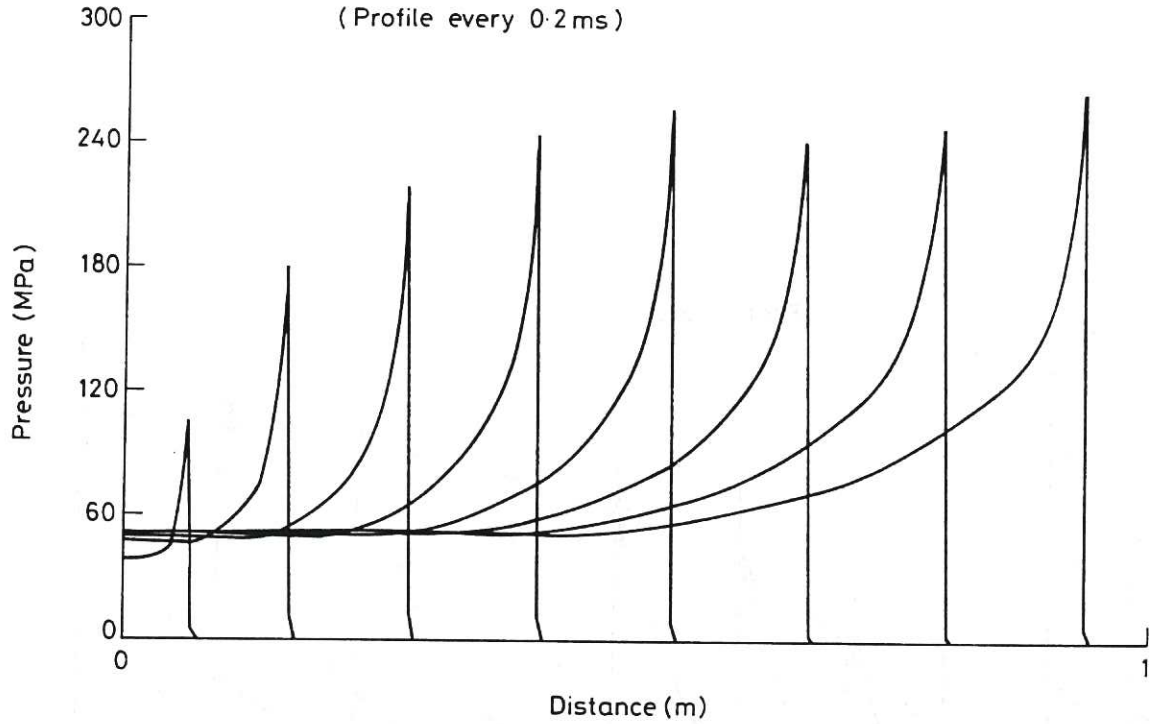

Fig. 6 Development of the pressure profile for a cylindrical geometry

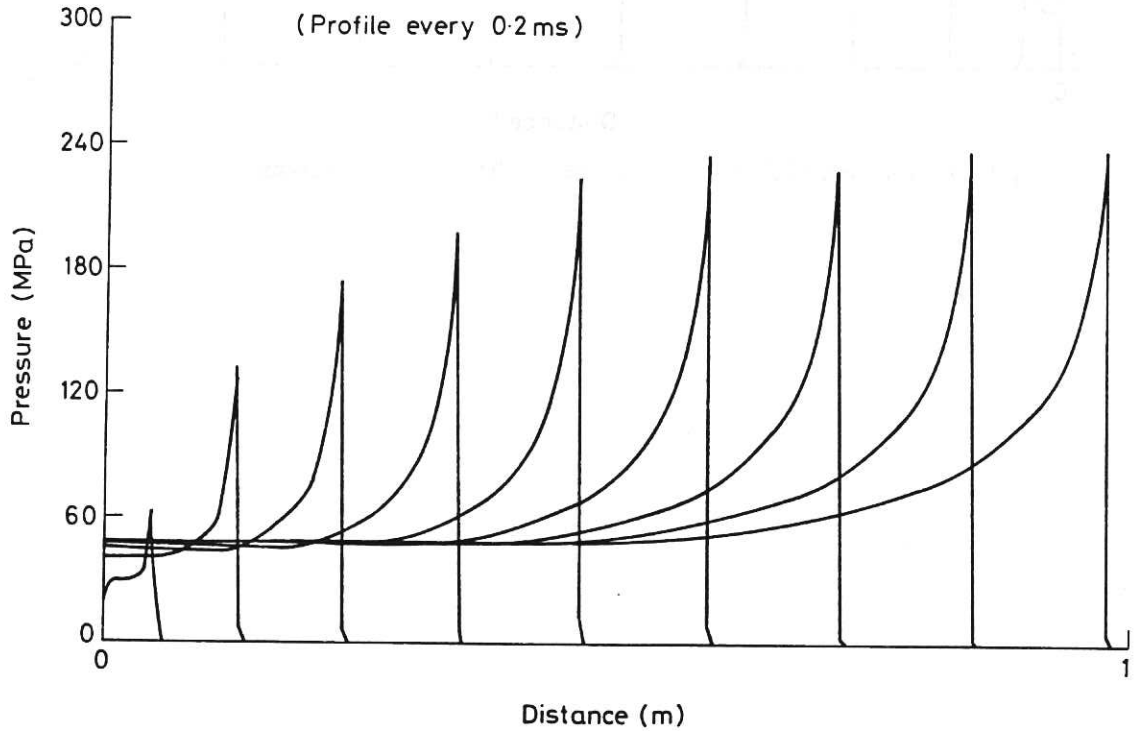

Fig. 7 Development of the pressure profile for a spherical geometry

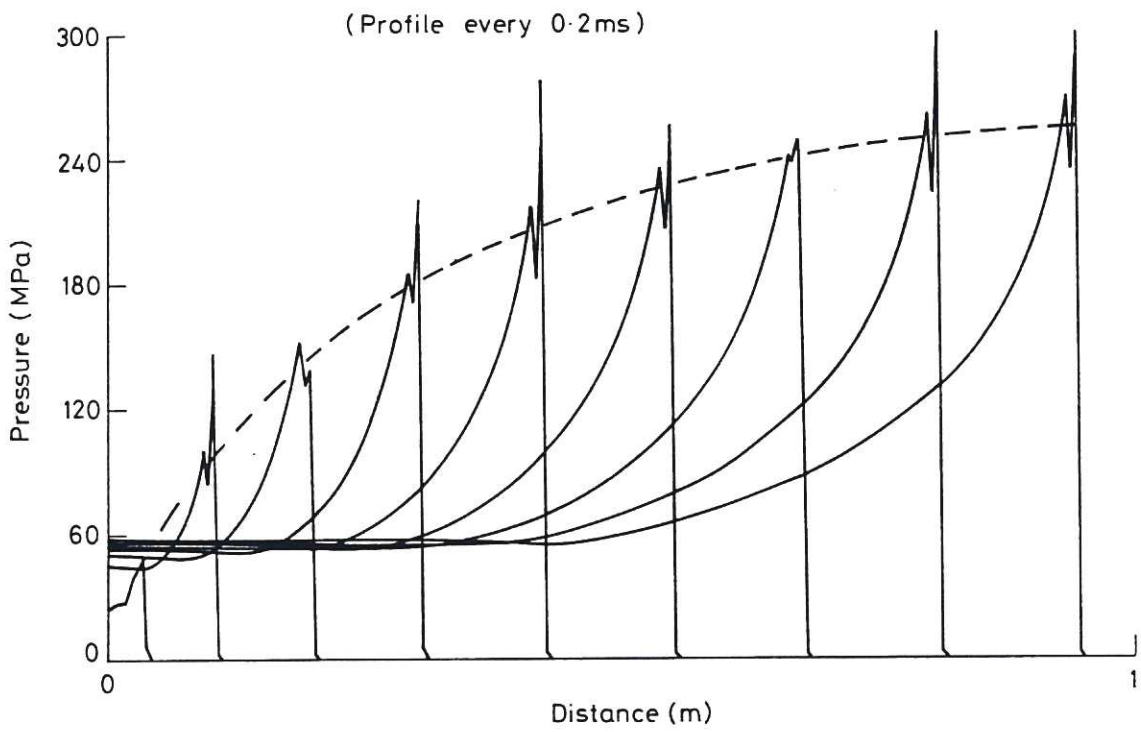

Fig. 8 Development of the pressure profile for the reduced heat transfer rate case